

Drastic Improvement of Air Stability in an n-type Doped Naphtalene-diimide Polymer by Thionation

Diego Nava^{†§}, Younghun Shin[‡], Matteo Massetti^{†§}, Xuechen Jiao^{¥□}, Till Biskup[#], Madan S. Jagadeesh[§], Alberto Calloni[§], Lamberto Duò[§], Guglielmo Lanzani^{†§}, Christopher R. McNeill[¥], Michael Sommer^{‡}, Mario Caironi^{†*}*

† Center for Nano Science and Technology @PoliMi, Istituto Italiano di Tecnologia, Via Pascoli
70/3, Milano 20133, Italy.

§ Politecnico di Milano, Dipartimento di Fisica, P.za L. da Vinci 32, Milano 20133, Italy

‡ Institut für Chemie, Technische Universität Chemnitz, Straße der Nationen 62, 09111
Chemnitz, Germany

¥ Department of Materials Science and Engineering, Monash University, Wellington Road,
Clayton, VIC, 3800, Australia

□ Australian Synchrotron, 800 Blackburn Road, Clayton, VIC, 3168, Australia

Institut für Physikalische Chemie, Albert-Ludwigs-Universität Freiburg, Albertstraße 21,
79104 Freiburg, Germany

* Mario Caironi: mario.caironi@iit.it

* Michael Sommer: michael.sommer@chemie.tu-chemnitz.de

Abstract

Organic thermoelectrics are attractive for the fabrication of flexible and cost-effective thermoelectric generators (TEGs) for waste heat recovery, in particular by exploiting large-area printing of polymer conductors. Efficient TEGs require both p- and n-type conductors: so far, the air instability of polymer n-type conductors, which typically lose orders of magnitude in electrical conductivity (σ) even for short exposure time to air, has impeded processing under ambient conditions. Here we tackle this problem in a relevant class of electron transporting, naphthalene-diimide co-polymers, by substituting the imide oxygen with sulphur. n-type doping of the thionated co-polymer gives rise to a higher σ with respect to the non-thionated one, and most importantly, owing to a reduced energy level of the lowest-unoccupied molecular orbital, σ is substantially stable over 16 h of air exposure. This result highlights the effectiveness of chemical tuning to improve air-stability of n-type solution-processable polymer conductors and shows a path towards ambient large-area manufacturing of efficient polymer TEGs.

Keywords: polymer conductors, n-type doping, organic thermoelectrics, air stability, conjugated polymers

Introduction

Energy harvesting with organics sees its most mature example in organic solar cells, which enables lightweight and large-area solar energy converters suitable for distributed energy generation.^{1,2} Organic materials could also support the development of other energy harvesting and scavenging³ devices that necessitate cost-competitive technologies to be economically viable, such as thermoelectric generators (OTEGs), that could be employed to supply power to low-consumption distributed and/or portable electronic devices. At the same time, such development could lead to custom-shaped active coolers,^{4,5} facilitating their integration into existing electronic appliances. One of the most appealing paths towards such applications is to make use of solution-processed organic compounds in order to enable mass-printed OTEGs, thus drastically limiting production costs. Yet, the development of organic thermoelectrics is far less mature than photovoltaics, with critical shortfalls in fundamental knowledge regarding the thermoelectric properties of conjugated molecule-based films,^{6,7} available materials,⁸⁻¹⁰ processing¹¹⁻¹³ and device engineering.¹⁴⁻¹⁸

The efficiency of the conversion of a heat flux into a current by thermoelectric (TE) materials can be related to the dimensionless material figure of merit zT , defined as:

$$(1) \quad zT = \frac{S^2 \sigma}{\kappa} T$$

where σ is the electrical conductivity, S is the Seebeck coefficient and κ is the thermal conductivity.

One of the most attractive characteristics of organic conductors or doped organic semiconductors is their low κ , typically below $1 \text{ Wm}^{-1} \text{ K}^{-1}$,^{9,19} as a result of the suppression of the phonon component in the thermal conductivity due to the intrinsic structural disorder.²⁰ A common strategy therefore to improve TE properties of organic semiconductors is to improve the numerator of zT , namely the power factor (PF).

$$(2) \quad PF = S^2\sigma \text{ [Wm}^{-1}\text{ K}^{-2}\text{]}$$

Since in their pristine form conjugated organic materials are typically insulators or semiconductors with low background conductivity, doping is necessary to achieve suitable electrical conductivity.²¹ Thus, tuning the doping level, namely modulating the charge carrier density, is a key aspect for optimizing PF and zT values.²² In organic semiconductors the doping process relies on the addition of sub-stoichiometric amounts of a redox-active species to the host semiconductor matrix. The dopant, which is a molecular species or a salt,^{23,24} donates an electron to the host (n-doping) or accepts an electron from the host, leaving a hole behind (p-doping) as a consequence either of direct charge-transfer,²⁵⁻²⁸ or of an indirect process. For example, proton transfer from acids or hydride transfer can lead to p-type and n-type doping, respectively.²⁹

For the realization of an efficient thermoelectric device, complementary p-type and n-type conducting materials with high PF are needed at the same time.³⁰ While solution processable organic p-type materials having a PF in excess of $100 \mu\text{Wm}^{-1} \text{K}^{-2}$ have been demonstrated,³¹⁻³⁴ the major limitations are ascribable to n-type materials, for which examples combining high electrical conductivity and solution processability are very scarce. A further strong limitation for n-type materials arises from their air instability, which precludes ambient processing of OTEGs and impose severe constraints regarding devices encapsulation.³⁵

To overcome this issue, both the dopant and the semiconductor must be air-stable. With regard to the dopant, adopting species with very low ionization energy to induce an electron transfer to the host semiconductor is critical, because the donating molecule is very prone to redox reactions with species in the atmosphere.³⁶ This is the reason why the hydride transfer scheme proposed by Bao and co-workers from ambient stable benzimidazole derivatives, such as 4-(1,3-dimethyl-2,3-dihydro-1H-benzimidazol-2-yl)-N,N-dimethylaniline (N-DMBI) and 4-(1,3-Dimethyl-2,3-

dihydro-1H-benzoimidazol-2-yl)-N,N-diphenylaniline (N-DPBI), immediately gained interest.³⁷ Chabinyk and co-workers reported a maximum conductivity of σ 10^{-3} Scm⁻¹ for poly{[N,N'-bis(2-octyldodecyl)-naphthalene-1,4,5,8-bis(dicarboximide)-2,6-diyl]-alt-5,5'-(2,2'-bithiophene)}, here abbreviated as PNDIT2 (Figure 1a), doped with N-DMBI.³⁸ Koster and co-workers^{39,40} recently explored a benzimidazole derivative to dope a modified fullerene, both tailored with hydrophilic triethylene glycol type side chains, achieving an electrical conductivity of 2.05 Scm⁻¹ and a *PF* of 19.1 μ W m⁻¹ K⁻², one of the highest reported for solution processable n-type materials. Pei and co-workers⁴¹ reported a series of BDPPV n-type conjugated polymers with low lying LUMO levels and very high *PF* values up to 28 μ W m⁻¹ K⁻². However, all the previous systems did not exhibit air stability or at least this aspect was not investigated. Generally, it is assumed that ambient stability of n-type conductivity can be achieved using materials with a LUMO energy level more negative than -3.9 eV.⁴²⁻⁴⁶

The lowering of the LUMO energy of the semiconductor can be obtained by diverse modifications of the electron withdrawing cores such as in naphthalene diimide (NDI) based co-polymers, one of the most studied class of n-type materials⁴⁷⁻⁵⁵ With the core positions being partially blocked in PNDIT2 by the comonomer, the strategy of lowering the LUMO by replacing the imide group by a mono-thioimide group, known as thionation, appears highly suitable for the development of stable n-doped small molecule NDIs⁵⁶⁻⁵⁹ and NDI-based polymers.^{60,61}

Here we make use of thionated PNDIT2, referred to as 2S-*trans*-PNDIT2 (Figure 1b) in which two carbonyl oxygens are substituted by sulphur with full *trans*-regioselectivity.⁶¹ 2S-*trans*-PNDIT2 exhibits a lower LUMO level compared to PNDIT2 which enables a drastically improved stability of n-type electrical conductivity at ambient conditions. When doped with N-DPBI (Figure 1c), σ is as high as $6 \cdot 10^{-3}$ Scm⁻¹, with an improved power factor with respect to PNDIT2, reaching

$4.9 \cdot 10^{-2} \mu\text{Wm}^{-1}\text{K}^{-2}$. Importantly, while doped PNDIT2 films lose several orders of magnitude of σ within 200 minutes, reaching almost the low conductivity of the undoped film, the conductivity of 2S-*trans*-PNDIT2 decreases by only a factor of two after 16 hours of continuous air exposure.

Materials

The herein used 2S-*trans*-PNDIT2 was obtained from the educt PNDIT2 using Lawesson's reagent as previously published.⁶¹ This PNDIT2 has a molecular weight from size exclusion chromatography (SEC) $M_{n,SEC}/M_{w,SEC} = 12/19$ kg/mol, and was also used as reference herein. The molecular weight of 2S-*trans*-PNDIT2 obtained by SEC under the same conditions was $M_{n,SEC}/M_{w,SEC} = 8/355$ kg/mol. However, for an equal chain length of the two materials it is apparent that the molar mass of 2S-*trans*-PNDI must be slightly higher than that of the corresponding educt PNDIT2. In fact molar mass determination by SEC is not straightforward here, as also seen by the very high M_w values caused by aggregation. We therefore made additional use of NMR end group analysis, which gives a $DP_{n,NMR}$ of 8.7 for PNDIT2 (and the same value for 2S-*trans*-PNDIT2).⁶¹ From the masses of the repeat units and an O/S conversion of 96 % for 2S-*trans*-PNDIT2, we estimate absolute number average molecular weights $M_{n,NMR}$ of 8.6 and 8.9 kg/mol for PNDIT2 and 2S-*trans*-PNDIT2, respectively.

Optical and Electrical Properties

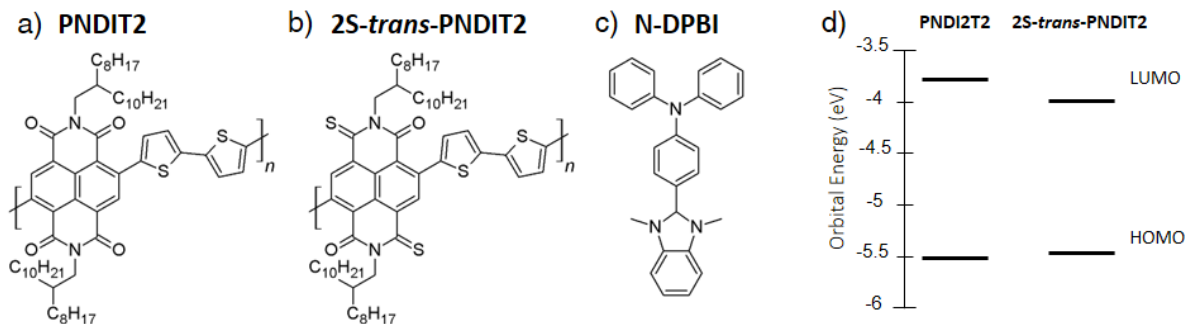


Figure 1. Chemical structures of a) PNDIT2, b) the thionated derivative 2S-*trans*-PNDIT2, c) the hydride dopant N-DPBI. d) Energy diagram for frontier energy orbitals of both co-polymers obtained from cyclic voltammetry and absorption in solution.

The effect of the substitution of the imide oxygen atoms with sulphur atoms is clearly visible from the UV-visible absorption spectra (see Supporting Information, SI, Figure S1)⁶¹. Comparing the spectra of the PNDIT2 and 2S-*trans*-PNDI, a strong red-shift of ≈ 100 nm in the absorption on-set is observed for the latter, indicating a significant reduction of the optical energy gap. Since the HOMO is mostly located on the thiophene moieties,⁶² while the LUMO is localized on the naphthalene-diimide unit,⁶³ the energy gap reduction should be ascribable to a deeper LUMO energy level as an effect of thionation. This is confirmed by cyclic voltammetry measurements (Figure S2), as reported by Shin *et. al.*⁶¹ By combining optical data and electrochemical data, following the methodology described in the SI, we can obtain a first estimation of the HOMO/LUMO energies (Figure 1d). For 2S-*trans*-PNDIT2 we extract energy values of -5.47 eV for the HOMO level and -3.96 eV for the LUMO, while for PNDIT2 we obtain -5.51 eV and -3.75 eV respectively for the HOMO and the LUMO level. As expected, thionation of the acceptor

moiety mostly reduces the LUMO level of 2S-*trans*-PNDIT2, while leaving the HOMO level substantially unperturbed.

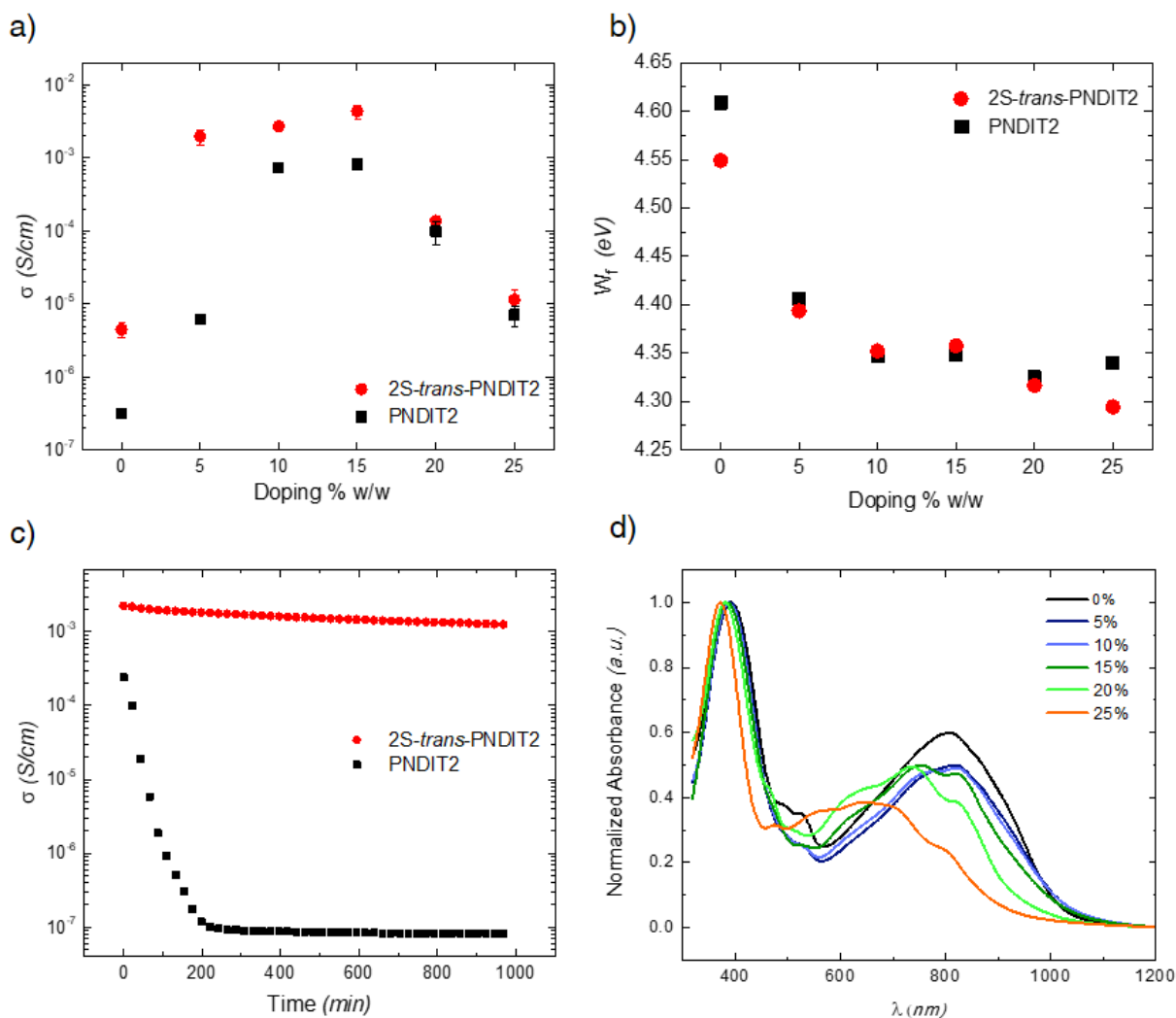


Figure 2. a) Electrical conductivity of 2S-*trans*-PNDIT2 (red dots) and PNDIT2 (black squares) thin films as a function of the N-DPBI dopant concentration. Each data point is an average of at least four devices, vertical error bars represent the standard deviation. b) Work function plot for 2S-*trans*-PNDIT2 (dots) and PNDIT2 (squares) as a function of doping concentration. c) Time dependence of the electrical conductivity of non-encapsulated thin films of 2S-*trans*-PNDIT2 (red

dots) and PNDIT2 (black squares), with 15 % w/w N-DPBI, upon ambient air exposure. d) UV-Vis-NIR thin film absorption spectra of 2S-*trans*-PNDIT2 doped with different w/w concentration of N-DPBI.

In order to dope the polymer films, we selected N-DPBI. Following the procedure reported by Schlitz *et al.* for PNDIT2,³⁸ we added N-DPBI directly to the 2S-*trans*-PNDIT2 toluene solution at various concentrations, from 5 % to 25 % by weight, and deposited a 40 nm thick film by spin-coating. We applied the same doping procedure to PNDIT2 as a reference.

In its pristine, undoped state, the 2S-*trans*-PNDIT2 film shows an electrical conductivity of $(4\pm 2)\cdot 10^{-6}$ Scm⁻¹. For undoped PNDIT2, a value that is one order of magnitude lower is found $(3\pm 1)\cdot 10^{-7}$ Scm⁻¹. This is in agreement with electron spin resonance (ESR) spectroscopy data indicating the presence of unpaired electrons in 2S-*trans*-PNDIT2, but not in PNDIT2 (Figure S11). After the addition of only 5 % w/w of N-DPBI, the conductivity of 2S-*trans*-PNDIT2 films drastically increases by more than two orders of magnitude, reaching $(2.0\pm 0.1)\cdot 10^{-3}$ Scm⁻¹. An increase of the doping concentration above 5 % w/w, at first leads to a small increase of σ , reaching a maximum value of $(5.9\pm 0.2)\cdot 10^{-3}$ Scm⁻¹ at 15 % w/w of N-DPBI. A further increase in dopant concentration is then detrimental for the electrical conductivity. A similar dependence of σ on dopant concentration was observed for PNDIT2 reference films, in good agreement with literature,^{38,64-66} where the maximum σ of $(1.2\pm 0.2)\cdot 10^{-3}$ Scm⁻¹, achieved at 15% w/w, is five times lower than for 2S-*trans*-PNDIT2. The difference in σ between the two systems is much stronger at low doping concentration: at 5 % w/w, σ is 330 times higher in the thionated sample than in the parent co-polymer, and even two times higher than the maximum electrical conductivity achieved at 15 % w/w in PNDIT2.

The effect of doping was also monitored by measuring the work function (W_f) by the Kelvin Probe technique (Figure 2b). Undoped films of 2S-*trans*-PNDIT2 feature a lower W_f , in agreement with an increased number of excess electrons already seen with ESR. With increasing dopant concentration, W_f reduces from 4.55 eV in the pristine film to 4.35 eV in the doped film at 10 % w/w concentration, where it reaches a plateau; a further increase in the doping concentration does not lead to an appreciable reduction of the work function as detectable by our Kelvin Probe setup. X-ray photoemission spectroscopy (XPS) was used to certify the presence of dopant molecules and to assess their chemical state. In particular, in the case of doped 2S-*trans*-PNDIT2 films, we detected the spectroscopic features of oxidized N-DPBI molecules (Figure S4 in SI and details therein).

Besides the difference in σ , what is remarkable is the difference in stability of the electrical conductivity between the two systems when films are directly exposed to ambient air. Figure 2c reports σ as a function of the ambient air exposure time, at room temperature and relative humidity of about 50 %, for both materials at a doping concentration of 15 % w/w. The electrical conductivity of PNDIT2 rapidly drops, reaching almost the pristine film value after 200 minutes. Such strong instability basically prevents any ambient processing of this doped system and its use for OTEGs fabrication. On the contrary, the electrical conductivity of 2S-*trans*-PNDIT2 remains within the same order of magnitude of its initial value for as long as 16 hours of air exposure, showing only a reduction factor slightly lower than 2. Similar behaviour in air stability was observed in 2S-*trans*-PNDIT2 for 5% w/w and 10% w/w doping concentrations (Figure S10). We assign the enhanced stability to the lower LUMO level in 2S-*trans*-PNDIT2 that allows electrons to relax at energy levels less prone to redox processes in ambient air. This is an unprecedented stability for doped n-type organic materials, and would clearly leave room for ambient processing

of organic thermoelectric devices, strongly desirable in case of high-throughput printing processes, before encapsulation.⁴⁶

It is interesting to note that the field-effect mobility as measured in bottom-contact, top-gate field-effect transistors based on the pristine thin films, is higher for PNDIT2 than for 2S-*trans*-PNDIT2, reaching the values of $0.30 \pm 0.02 \text{ cm}^2 \text{V}^{-1} \text{s}^{-1}$ and $0.05 \pm 0.01 \text{ cm}^2 \text{V}^{-1} \text{s}^{-1}$, respectively (details reported in Figure S5).⁶¹ The bulk mobility of doped films and the mobility of field-effect transistors are not directly comparable.^{67,68} However, since the charge density achieved in the field-effect device is of the same order of magnitude of the one achieved in doped films,^{69,70} it is reasonable to expect that the higher conductivity in doped 2S-*trans*-PNDIT2 films (Figure 3a) is not caused by an improved electron mobility.

Thus, the improved σ in doped 2S-*trans*-PNDIT2 films suggests a higher efficacy of the doping process leading to a higher charge density. The ESR signal intensity for 2S-*trans*-PNDIT2 at 15% w/w doping was two times higher than the one of PNDIT2, clearly confirming a higher carrier density (Figure S12).

To further investigate the factors that cause the higher conductivity of 2S-*trans*-PNDIT2, we followed the doping process through optical absorption and structural measurements on thin films as a function of doping concentration. Figure 2d shows the UV-vis optical absorption spectra evolution of 2S-*trans*-PNDIT2 with doping concentration. The pristine film has a broad band from 600 to 1000 nm, with a peak around 810 nm. The strong red-shift with respect to the spectrum of molecularly dissolved chains in chloronaphthalene solution is due to aggregation.⁶² At low doping concentration (5 and 10 % w/w), the intensity of the low energy band reduces, with the appearance of a stronger component at around 600 nm in the 10 % w/w case, indicating an increased presence of a non-aggregated, amorphous phase. For a doping concentration above 15 % w/w, the shoulder

between 800 nm and 1000 nm becomes increasingly suppressed in favour of the non-aggregated component at 600 nm and the ratio between the 750 nm and 830 nm peaks rapidly increases. Overall, the evolution of the UV-Vis spectra with doping concentration suggests that the dopant molecule suppresses chain-chain interactions of *2S-trans*-PNDIT2, resulting in an increased amorphous component. Differently, in case of doped PNDIT2 (Figure S3), an increasing doping concentration mainly causes a reduction of the intensity of the 600 – 800 nm band while keeping the ratio of vibronic bands constant up to 15 % w/w. Higher doping concentrations did not lead to further modification of the UV-vis spectra indicating a weaker interaction of the dopant with PNDIT2.

Optical absorption measurements therefore suggest a structural evolution in *2S-trans*-PNDIT2 films with doping.

Morphological Characterization

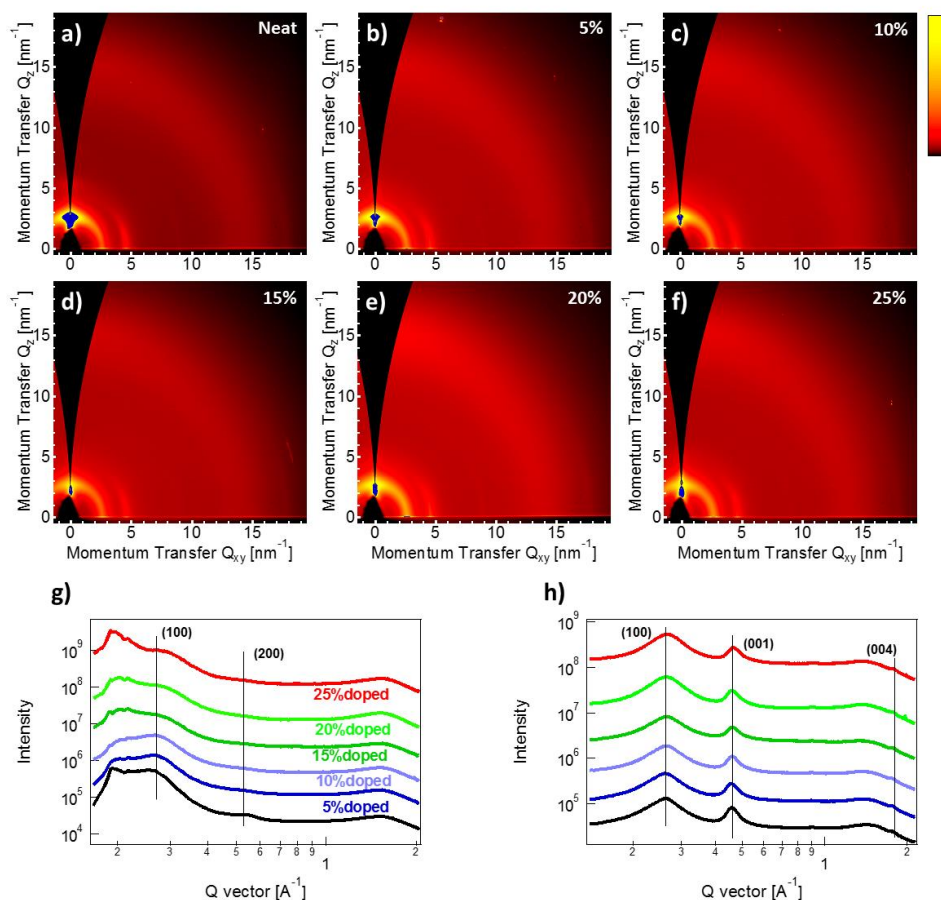


Figure 3. Two-dimensional data plots of GIWAXS measurements of 2S-*trans*-PNDIT2 films for different doping concentrations, from a) to f): 0, 5, 10, 15, 20 and 25 % w/w. Corresponding one-dimensional g) out-of-plane and h) in-plane GIWAXS profiles.

The microstructure of these thin films was further investigated by grazing incidence wide angle X-ray scattering (GIWAXS). Comparing the GIWAXS patterns of films of undoped 2S-*trans*-PNDIT2 (Figure 3a) and PNDIT2 (Figure S4a), 2S-*trans*-PNDIT2 exhibits less microstructural order. Although lamellar packing and backbone repeat distance are similar, 2S-*trans*-PNDIT2 exhibits a lower degree of crystalline order evidenced by broader peaks with an apparent absence

of a π - π stacking peak.⁶¹ Furthermore, films of 2S-*trans*-PNDIT2 exhibit more orientational disorder, with crystallites exhibiting a broad orientational distributions from face-on to edge-on. Thus, thionation of PNDIT2 reduces microstructural order which may explain in part the reduced field-effect mobilities of 2S-*trans*-PNDIT2 compared to PNDIT2.⁶¹ With increasing doping concentration, 2S-*trans*-PNDIT2 displays a further decrease in order. Undoped films (Figure 3a), while exhibiting a range of molecular orientations, show a slight preference for edge-on orientation, evidenced by the first-order lamellar stacking peak, (100), at $\sim 2.5 \text{ nm}^{-1}$ along the out-of-plane direction, with a second-order peak, (200), also observable at $\sim 5 \text{ nm}^{-1}$ (see also in-plane traces in Figure 3g). With increased doping, this edge-on population is less evident, with no preference for face-on or edge-on orientation in films with 15% w/w doping and above. The lamellar stacking d-spacings for the remaining crystalline population appear unaffected (Figure 3h), indicating that the dopant molecule is not intercalating within the side-chains. Since a π - π stacking peak is not clearly present, it is not possible to say whether the dopant molecules are intercalating between two stacked backbones. A strikingly different behaviour with doping is observed for the parent PNDIT2 (Figure S6). As-cast PNDIT2 films exhibit a pronounced edge-on stacking of chains, with four orders of lamellar stacking peaks evident. We note that this is unusual for PNDIT2 films, likely due to the low molecular weight adopted in this case. With doping, the PNDIT2 appears to become more ordered, evidenced by narrower lamellar stacking and backbone peaks, unlike for 2S-*trans*-PNDIT2, where the doping induces more structural disorder. Similar to 2S-*trans*-PNDIT2, the observed d-spacings are unaffected by doping, indicating that the dopant is not intercalating within the crystals. In both cases no scattering from the dopant crystals is appearing, with the second-order lamellar stacking no longer evident.

Taking together the results from optical absorption and GIWAXS, we conclude that N-DPBI dopant is predominantly incorporated in the amorphous portion of 2S-*trans*-PNDIT2 films and

does not substantially alter the molecular packing motif of the crystals that do form. Since 2S-*trans*-PNDIT2 features less microstructural order, miscibility with N-DPBI is likely increased. Addition of N-DPBI thus hinders the crystallisation of 2S-*trans*-PNDIT2, in a similar fashion to the way fullerene molecules such as PCBM hinders the crystallisation of poly(3-hexylthiophene) in as-cast P3HT/PCBM blends.⁷¹ A higher 2S-*trans*-PNDIT2 amorphous fraction in blends with N-DPBI is consistent with the appearance of a non-aggregated absorption component in UV-vis spectra with increasing dopant concentration. A reduction in the extension of polymer crystallites upon dopant addition results in a smaller fraction of the film which is precluded to the dopant and can explain the higher conductivity at 5 % w/w doping with respect to PNDIT2, despite a lower field-effect mobility. Still, at high dopant concentration, miscibility of the two components is a limiting factor on the doping efficacy, with an obvious phase separation, also evidenced by AFM topography measurements (Figure S7).³⁸ For PNDIT2 films, the high tendency of PNDIT2 chains to crystallise means that there is a lower fraction of chains which are able to interact with the dopant on the molecular level.

Seebeck Measurements

The Seebeck coefficient of the two doped co-polymers was finally measured at 15% w/w. For 2S-*trans*-PNDIT2 thin films doped with N-DPBI at 15 % w/w, we obtained $S = -90 \pm 4 \mu\text{VK}^{-1}$, leading to a power factor of $4.9 \cdot 10^{-2} \mu\text{Wm}^{-1}\text{K}^{-2}$. The negative sign of the Seebeck is indicative of electrons being the majority carriers. PF is significantly higher than the maximum value we can obtain with PNDIT2, where we extract $PF = 1.2 \cdot 10^{-2} \mu\text{Wm}^{-1}\text{K}^{-2}$ under the same conditions, in line with the results reported by Wang et al.⁶⁴ Thus, thionation of PNDIT2 is not only effective in drastically improving the air stability of doped NDI-based copolymer films but also in improving the overall thermoelectric performance. The improved electrical conductivity, owing to a more favourable

interaction of the dopant and the polymer, enables a four-fold improvement in power factor to be realised.

Conclusions

In conclusion, we have reported an effective strategy to strongly improve ambient stability of n-type doped NDI-based copolymers. The lower LUMO level of *2S-trans*-PNDIT2 reduces the reactivity of excess electrons in air significantly. *2S-trans*-PNDIT2 also has a weaker tendency to crystallise compared to PNDIT2, which promotes favourable molecular interactions between the polymer backbone and the dopant. Doping of *2S-trans*-PNDIT2 with the stable N-DPBI molecule produces a strong increase of electrical conductivity already at a doping concentration as low as 5 % w/w, and the *PF* extracted at maximum σ is four times higher than PNDIT2. The stability of σ for doped *2S-trans*-PNDIT2 films completely exposed to air is unprecedented for n-type conductivity in polymers. *2S-trans*-PNDIT2 shows a reduction in conductivity of less than a factor of two over 16 h of continuous air exposure, compared to the three orders of magnitude loss measured in the first hour only for PNDIT2. Such a pronounced improvement demonstrates that inherent environmental stability of n-type doped polymer conductors can be largely controlled through the proper design of the conjugated semiconductor system. This result is an important step towards stable n-type doped polymers, which more favourably allow ink formulation for large-area manufacturing through scalable printing technologies, which finally may enable high throughput fabrication of low-cost and efficient organic thermoelectric generators under ambient conditions based on thermocouples combining n-type and p-type materials.

Experimental Section

Materials

PNDIT2 and 2S-*trans*-PNDIT2 were synthesized according to published procedures.^{61,62} N-DPBI 4-(1,3-Dimethyl-2,3-dihydro-1H-benzoimidazol-2-yl)-N,N-diphenylaniline was purchased from Sigma-Aldrich and used as received.

Solutions preparation

Both copolymers were dissolved in toluene at a concentration of 5 g/l and stirred at 80 °C for 4 hours. N-DPBI solutions were prepared at concentrations of 3, 5 and 8 g/l and used after \approx 12 h of dissolution at room temperature. Aliquots of polymer and dopant solution were mixed and stirred for 10 min. at room temperature just before the deposition.

Thin films preparation

Low alkali 1737F Corning glass was used as substrate. The substrates were cleaned in ultrasonic bath of Milli-Q water, acetone and isopropyl alcohol, 10 minutes for each step, and exposed to O₂-plasma at 100 W for 10 minutes. Electrodes were obtained by thermal evaporation, through a shadow mask, of a 1.5nm thick Cr adhesion layer and 25 nm thick Au film. For Field Effect Transistor bottom electrodes were patterned by a lift-off photolithographic process, defining a 20 μ m channel length and a 2 mm channel width. Metals were deposited by thermal evaporation: 1.5 nm thick Cr, as adhesion layer and 20 nm thick Au. Thin polymer films were spin cast from solutions onto pre-patterned substrates, in a nitrogen-filled glovebox at 1000 rpm for 60 s, and annealed at 150 °C for 2 hours in inert atmosphere. For Field Effect Transistor devices after the polymer thin film deposition, a dielectric layer with thickness of 600 nm was obtained by spin-coating a 80 g/l PMMA solution in n-Butyl acetate at 1300 rpm for 60 s under nitrogen atmosphere, followed by an annealing at 80 °C for 1 h in inert atmosphere. The 40 nm thick gate contact was obtained by thermal evaporation of Al through a shadow mask.

Electrical characterization

The I-V curves and the FET characteristics were measured at room temperature in a N₂ atmosphere, or in ambient air, Figure 2c, on a Wentworth Laboratories probe station with a semiconductor device analyser (Agilent B1500A). The electrical conductivity was extracted through the linear fit of the I-V characteristics, Figure S8. The saturation mobility values were extracted using the gradual-channel approximation.

UV-Vis-NIR measurements

UV-Vis-NIR measurements were carried out on a Perkin Elmer λ 1050 spectrophotometer, using a tungsten lamp as source.

Kelvin Probe measurements

Kelvin Probe measurements were done in air with a KP Technology Ambient air Kelvin Probe instrument. For the extraction of the work function we used the multiple single-point measurements mode. The work function of the sample was obtained by adding to the measured work function value the Contact Potential Difference (CDP) of the tip, determined with an initial calibration on standard gold substrate.

ESR measurements

Films were prepared under inert atmosphere by drop-casting 20 μ L solution (concentration of 5 g/l) onto synthetic quartz glass substrates (Ilmasil PS, QSIL GmbH) with dimensions of 3 \times 25 mm, followed by annealing at 150 $^{\circ}$ C for 120 min after films were dried completely. The annealed films were placed into synthetic quartz glass tubes (Ilmasil PS, QSIL GmbH) with 3.8 mm outer and 3.0 mm inner diameter and the tubes sealed afterwards. ESR spectra were

recorded at room temperature on an Elexsys 580 (Bruker Biospin GmbH) spectrometer equipped with a 4119HS-W1 (Bruker) cavity. Microwave frequency: 9.800 GHz; microwave power: 150 μ W (30 dB attenuation, 150 mW source power); modulation frequency: 100 MHz; modulation amplitude: 0.1 mT.

GIWAXS Characterization

Grazing-incidence wide-angle X-ray scattering (GIWAXS) was performed at the SAXS/WAXS beamline at the Australian Synchrotron.⁷² 11 keV photons were used with scattering patterns recorded on a Dectris Pilatus 1M detector. Images shown were acquired at an incident angle close to the critical angle. Such images were chosen from a series of recorded 2D patterns with incident X-ray angle varying from 0.05° to 0.25° in the step of 0.01°. The X-ray exposure time was 1 s such that no film damage was identified. The sample-to-detector distance was calibrated using a silver behenate sample. The results were analysed by an altered version of the NIKA 2D⁷³ based in IgorPro.

Atomic Force Microscopy

AFM polymer thin film samples were prepared using the same procedure describe in the experimental section. The surface morphology of the films was obtained with an Agilent 5500 Atomic Force Microscope operated in the Acoustic Mode.

Seebeck measurements

For the Seebeck measurements we employed a home-made set up described by Beretta et al.⁷⁴ The measurements were done in vacuum, at 10⁻⁴ mbar, to avoid convection phenomena and to preserve

the polymer electrical properties. In addition, the measurements were performed at a temperature of 45 °C, to have an electrical resistance below 10 MΩ, which is our system threshold for a correct measurement of the Seebeck coefficient. Before the measurement, we annealed overnight the samples at 90 °C, to avoid any possible thermal effects and/or thermal hysteresis during the thermoelectric measurements.

Supporting Information Available:

Optical and electrochemical characterization of both co-polymers, extraction procedure of HOMO and LUMO levels, XPS analysis, Field Effect Transistors characterization, GIWAXS characterization of PNDIT2, AFM images and Current/Voltage plots, ESR spectra.

Notes

The authors declare no competing financial interest.

Acknowledgements

The authors thanks F. Scuratti for help with AFM measurements. M. C. and D. N. acknowledge the European Research Council (ERC) for the financial support, under the European Union's Horizon 2020 research and innovation programme 'HEROIC', grant agreement 638059. Y. S. and M. S. acknowledge the Deutsche Forschungsgemeinschaft (SO 1213/ 8-1) for funding. T.B. acknowledges the Deutsche Forschungsgemeinschaft (TB 1249/3-1) for funding. This work was performed in part at the SAXS/WAXS beamline at the Australian Synchrotron, part of ANSTO. C.R.M. acknowledges support from the Australian Research Council (DP170102145).

References

- (1) Huang, Y.; Kramer, E. J.; Heeger, A. J.; Bazan, G. C. Bulk Heterojunction Solar Cells: Morphology and Performance Relationships. *Chem. Rev.* **2014**, *114*, 7006–7043.
- (2) Mazziio, K. A.; Luscombe, C. K. The Future of Organic Photovoltaics. *Chem. Soc. Rev.* **2014**, *44*, 78–90.
- (3) LeBlanc, S. Thermoelectric Generators: Linking Material Properties and Systems Engineering for Waste Heat Recovery Applications. *Sustain. Mater. Technol.* **2014**, *1*, 26–35.
- (4) Bahk, J.-H.; Fang, H.; Yazawa, K.; Shakouri, A. Flexible Thermoelectric Materials and Device Optimization for Wearable Energy Harvesting. *J. Mater. Chem. C* **2015**, *3*, 10362–10374.
- (5) Zhao, D.; Tan, G. A Review of Thermoelectric Cooling: Materials, Modeling and Applications. *Appl. Therm. Eng.* **2014**, *66*, 15.
- (6) Zhang, Q.; Sun, Y.; Xu, W.; Zhu, D. What To Expect from Conducting Polymers on the Playground of Thermoelectricity: Lessons Learned from Four High-Mobility Polymeric Semiconductors. *Macromolecules* **2014**, *47*, 609.
- (7) Culebras, M.; Gómez, C. M.; Cantarero, A. Review on Polymers for Thermoelectric Applications. *Materials*. **2014**, *6*, 6701–6732.
- (8) Sun, Y.; Sheng, P.; Di, C.; Jiao, F.; Xu, W.; Qiu, D.; Zhu, D. Organic Thermoelectric Materials and Devices Based on p - and n -Type Poly (Metal 1 , 1 , 2 , 2-Ethenetetrathiolate) S. *Adv. Mater.* **2012**, *24*, 932–937.

- (9) Yan, H.; Sada, N.; Toshima, N. Thermal Transporting Properties of Electrically Conductive Polyaniline Films as Organic Thermoelectric Material. *J. Therm. Anal. Calorim.* **2002**, *69*, 881–887.
- (10) Kroon, R.; Kiefer, D.; Stegerer, D.; Yu, L.; Sommer, M.; Müller, C. Polar Side Chains Enhance Processability, Electrical Conductivity and Thermal Stability of a Molecularly p-Doped Polythiophene. *Adv. Mater.* **2017**, *29*, 35–37.
- (11) Kiefer, D.; Yu, L.; Fransson, E.; Gómez, A.; Primetzhofer, D.; Amassian, A.; Campoy-Quiles, M.; Müller, C. A Solution-Doped Polymer Semiconductor: Insulator Blend for Thermoelectrics. *Adv. Sci. news* **2017**, *4*, 1600203.
- (12) Hong, C. T.; Kang, Y. H.; Ryu, J.; Cho, S. Y.; Jang, K. Spray-Printed CNT/P3HT Organic Thermoelectric Films and Power Generators. *J. Mater. Chem. A* **2015**, *3*, 21428–21433.
- (13) Glaudell, A. M.; Cochran, J. E.; Patel, S. N.; Chabynyc, M. L. Impact of the Doping Method on Conductivity and Thermopower in Semiconducting Polythiophenes. *Adv. Energy Mater.* **2015**, *5*, 1401072.
- (14) Park, T.; Park, C.; Kim, B.; Shin, H.; Kim, E. Environmental Science Power Factors to Generate Electricity by the Touch of Fingertips. *Energy Environ. Sci.* **2013**, *6*, 788–792.
- (15) Lee, S. H.; Park, H.; Kim, S.; Son, W.; Cheong, I. W.; Kim, J. H. Transparent and Flexible Organic Semiconductor Nano Films with Enhanced Thermoelectric Efficiency. *J. Mater. Chem. A* **2014**, *2*, 7288–7294.
- (16) Rojas, J. P.; Singh, D.; Conchouso, D.; Arevalo, A.; Foulds, I. G.; Hussain, M. M. Stretchable Helical Architecture Inorganic-Organic Hetero Thermoelectric Generator. *Nano*

Energy **2016**, *30*, 691–699.

- (17) Menon, A. K.; Yee, S. K. Design of a Polymer Thermoelectric Generator Using Radial Architecture. *J. Appl. Phys.* **2016**, *119*, 055501.
- (18) Søndergaard, R. R.; Hosel, M.; Espinosa, N.; Jørgensen, M.; Krebs, F. C. Practical Evaluation of Organic Polymer Thermoelectrics by Large-Area R2R Processing on Flexible Substrates. *Energy Sci. Eng.* **2013**, *1*, 81–88.
- (19) Zhang, X.; Lu, X.; Zhen, Y.; Liu, J.; Dong, H.; Zhao, G.; He, P.; Wang, Z.; Jiang, L.; Hu, W. Synthesis and Aggregation-Induced Emissions of Thienyl Substituted Cyclobutene Derivatives. *J. Mater. Chem. C* **2014**, *2*, 5083.
- (20) Bubnova, O.; Khan, Z. U.; Malti, A.; Braun, S.; Fahlman, M.; Berggren, M.; Crispin, X. Optimization of the Thermoelectric Figure of Merit in the Conducting Polymer Poly (3, 4-Ethylenedioxythiophene). *Nat. Mater.* **2011**, *10*, 429–433.
- (21) Kroon, R.; Mengistie, D. A.; Kiefer, D.; Hynynen, J.; Ryan, J. D.; Yu, L.; Müller, C. Thermoelectric Plastics: From Design to Synthesis, Processing and Structure–property Relationships. *Chem. Soc. Rev.* **2016**, *45*, 6147–6164.
- (22) Russ, B.; Glauddell, A.; Urban, J.; L. Chabinye, M.; A. Segalman, R. Organic Thermoelectric Materials for Energy Harvesting and Temperature Control. *Nat. Rev. Mater.* **2016**, *1*, 16050.
- (23) Qi, Y.; Mohapatra, S. K.; Kim, S. B.; Barlow, S.; Marder, S. R. Solution Doping of Organic Semiconductors Using Air-Stable n-Dopants. *Appl. Phys. Lett.* **2012**, *100*, 083305.
- (24) Lu, G.; Blakesley, J.; Himmelberger, S.; Pingel, P.; Frisch, J.; Lieberwirth, I.; Salzmann, I.; Oehzelt, M.; Di Pietro, R.; Salleo, A.; Koch, N.; Neher, D. Moderate Doping Leads to High

- Performance of Semiconductor/Insulator Polymer Blend Transistors. *Nat. Commun.* **2013**, *4*, 1588.
- (25) Werner, A. G.; Li, F.; Harada, K.; Pfeiffer, M.; Fritz, T.; Leo, K. Pyronin B as a Donor for N-Type Doping of Organic Thin Films. *Appl. Phys. Lett.* **2003**, *82*, 4495–4497.
- (26) Li, F.; Werner, A.; Pfeiffer, M.; Leo, K.; Liu, X. Leuco Crystal Violet as a Dopant for N-Doping of Organic Thin Films of Fullerene C60. *J. Phys. Chem. B* **2004**, *108*, 17076–17082.
- (27) Werner, A.; Li, F.; Harada, K.; Pfeiffer, M.; Fritz, T.; Leo, K.; Machill, S. N-Type Doping of Organic Thin Films Using Cationic Dyes. *Adv. Funct. Mater.* **2004**, *14*, 255–260.
- (28) Chueh, C.-C.; Li, C.-Z.; Ding, F.; Li, Z.; Cernetic, N.; Li, X.; Jen, A. K.-Y. Doping Versatile N-Type Organic Semiconductors via Room Temperature Solution-Processable Anionic Dopants. *ACS Appl. Mater. Interfaces* **2017**, *9*, 1136–1144.
- (29) Lussem, B.; Riede, M.; Leo, K. Doping of Organic Semiconductors. *Phys. Status Solidi A* **2013**, *210*, 9–43.
- (30) Bubnova, O.; Crispin, X. Environmental Science Towards Polymer-Based Organic Thermoelectric Generators. *Energy Environ. Sci.* **2012**, *5*, 9345.
- (31) Kim, G.; Shao, L.; Zhang, K.; Pipe, K. P. Engineered Doping of Organic Semiconductors for Enhanced Thermoelectric Efficiency. *Nat. Mater.* **2013**, *12*, 719–723.
- (32) Toshima, N. Conductive Polymers as a New Type Of Thermoelectric Material. *Macromol. Symp.* **2002**, *186*, 81–86.
- (33) Zhang, K.; Zhang, Y.; Wang, S. Enhancing Thermoelectric Properties of Organic Composites through Hierarchical Nanostructures. *Sci. Rep.* **2013**, *3*, 3448.

- (34) Fan, Z.; Li, P.; Du, D.; Ouyang, J. Significantly Enhanced Thermoelectric Properties of PEDOT:PSS Films through Sequential Post-Treatments with Common Acids and Bases. *Adv. Energy Mater.* **2017**, *7*, 1602116.
- (35) Cowen, L. M.; Atoyo, J.; Carnie, M. J.; Baran, D.; Schroeder, B. C. Review — Organic Materials for Thermoelectric Energy Generation. *ECS J. Solid State Sci. Technol.* **2017**, *6*, 3080–3088.
- (36) Tietze, M. L.; Rose, B. D.; Schwarze, M.; Fischer, A.; Runge, S.; Blochwitz-Nimoth, J.; Lüssem, B.; Leo, K.; Brédas, J. L. Passivation of Molecular N-Doping: Exploring the Limits of Air Stability. *Adv. Funct. Mater.* **2016**, *26*, 3730–3737.
- (37) Naab, B. D.; Guo, S.; Olthof, S.; Evans, E. G. B.; Wei, P.; Millhauser, G. L.; Kahn, A.; Barlow, S.; Marder, S. R.; Bao, Z. Mechanistic Study on the Solution-Phase n-Doping of 1,3-Dimethyl-2-Aryl-2,3-Dihydro-1H-Benzoimidazole Derivatives. *J. Am. Chem. Soc.* **2013**, *135*, 15018–15025.
- (38) Schlitz, R. A.; Brunetti, F. G.; Glaudell, A. M.; Miller, P. L.; Brady, M. A.; Takacs, C. J.; Hawker, C. J.; Chabynyc, M. L. Solubility-Limited Extrinsic n-Type Doping of a High Electron Mobility Polymer for Thermoelectric Applications. *Adv. Mater.* **2014**, *26*, 2825–2830.
- (39) Liu, J.; Qiu, L.; Portale, G.; Koopmans, M.; ten Brink, G.; Hummelen, J. C.; Koster, L. J. A. N-Type Organic Thermoelectrics: Improved Power Factor by Tailoring Host–Dopant Miscibility. *Adv. Mater.* **2017**, *29*, 1701641.
- (40) Qiu, L.; Liu, J.; Alessandri, R.; Qiu, X.; Koopmans, M.; Havenith, R. W. A.; Marrink, S. J.; Chiechi, R. C.; Koster, L. J. A.; Hummelen, J. C. Enhancing Doping Efficiency by

- Improving Host-Dopant Miscibility for Fullerene-Based n-Type Thermoelectrics. *J. Mater. Chem. A* **2017**, *5*, 21234.
- (41) Shi, K.; Zhang, F.; Di, C.-A.; Yan, T.-W.; Zou, Y.; Zhou, X.; Zhu, D.; Wang, J.-Y.; Pei, J. Toward High Performance n-Type Thermoelectric Materials by Rational Modification of BDPPV Backbones. *J. Am. Chem. Soc.* **2015**, *137*, 6979–6982.
- (42) de Leeuw, D. M.; Simenon, M. M. J.; Brown, A. R.; Einerhand, R. E. F. Stability of N-Type Doped Conducting Polymers and Consequences for Polymeric Microelectronic Devices. *Synth. Met.* **1997**, *87*, 53–59.
- (43) Jousseme, B.; Sonmez, G.; Wudl, F. Acidity and Electronegativity Enhancement of C 60 Derivatives through Cyano Groups. *J. Mater. Chem.* **2006**, *16*, 3478–3482.
- (44) Boom, T. Van Der; Hayes, R. T.; Zhao, Y.; Bushard, P. J.; Weiss, E. A.; Wasielewski, M. R. Charge Transport in Photofunctional Nanoparticles Self-Assembled from Zinc 5,10,15,20-Tetrakis(Perylenediimide)Porphyrin Building Blocks. *J. Am. Chem. Soc.* **2002**, *124*, 9582–9590.
- (45) Di Pietro, R.; Fazzi, D.; Kehoe, T. B.; Sirringhaus, H. Spectroscopic Investigation of Oxygen- and Water-Induced Electron Trapping and Charge Transport Instabilities in n-Type Polymer Semiconductors. *J. Am. Chem. Soc.* **2012**, *134*, 14877.
- (46) Jones, B. A.; Facchetti, A.; Wasielewski, M. R.; Marks, T. J. Tuning Orbital Energetics in Arylene Diimide Semiconductors. Materials Design for Ambient Stability of n-Type Charge Transport. *J. Am. Chem. Soc.* **2007**, *129*, 15259–15278.
- (47) Naab, B. D.; Gu, X.; Kurosawa, T.; To, J. W. F.; Salleo, A.; Bao, Z. Role of Polymer

- Structure on the Conductivity of N-Doped Polymers. *Adv. Electron. Mater.* **2016**, *2*, 1600004.
- (48) Zhang, Y.; Phan, H.; Zhou, H.; Zhang, X.; Zhou, J.; Moudgil, K.; Barlow, S.; Marder, S. R.; Facchetti, A.; Nguyen, T. Q. Electron Transport and Nanomorphology in Solution-Processed Polymeric Semiconductor n-Doped with an Air-Stable Organometallic Dimer. *Adv. Electron. Mater.* **2017**, *3*, 1600546.
- (49) Yang, J.; Xiao, B.; Tajima, K.; Nakano, M.; Takimiya, K.; Tang, A.; Zhou, E. Comparison among Perylene Diimide (PDI), Naphthalene Diimide (NDI), and Naphthodithiophene Diimide (NDTI) Based n-Type Polymers for All-Polymer Solar Cells Application. *Macromolecules* **2017**, *50*, 3179–3185.
- (50) Nakano, K.; Nakano, M.; Xiao, B.; Zhou, E.; Suzuki, K.; Osaka, I.; Takimiya, K.; Tajima, K. Naphthodithiophene Diimide-Based Copolymers: Ambipolar Semiconductors in Field-Effect Transistors and Electron Acceptors with Near-Infrared Response in Polymer Blend Solar Cells. *Macromolecules* **2016**, *49*, 1752–1760.
- (51) Yang, J.; Chen, F.; Xiao, B.; Sun, S.; Sun, X.; Tajima, K.; Tang, A.; Zhou, E. Modulating the Symmetry of Benzodithiophene by Molecular Tailoring for the Application in Naphthalene Diimide-Based N-Type Photovoltaic Polymers. *Sol. RRL* **2018**, *2*, 1700230.
- (52) Zhou, E.; Nakano, M.; Izawa, S.; Cong, J.; Osaka, I.; Takimiya, K.; Tajima, K. All-Polymer Solar Cell with High near-Infrared Response Based on a Naphthodithiophene Diimide (NDTI) Copolymer. *ACS Macro Lett.* **2014**, *3*, 872–875.
- (53) Zhou, E.; Cong, J.; Hashimoto, K.; Tajima, K. Control of Miscibility and Aggregation via the Material Design and Coating Process for High-Performance Polymer Blend Solar Cells.

- Adv. Mater.* **2013**, *25*, 6991–6996.
- (54) Zhou, E.; Cong, J.; Wei, Q.; Tajima, K.; Yang, C.; Hashimoto, K. All-Polymer Solar Cells from Perylene Diimide Based Copolymers: Material Design and Phase Separation Control. *Angew. Chemie - Int. Ed.* **2011**, *50*, 2799–2803.
- (55) Bucella, S. G.; Luzio, A.; Gann, E.; Thomsen, L.; McNeill, C. R.; Pace, G.; Perinot, A.; Chen, Z.; Facchetti, A.; Caironi, M. Macroscopic and High-Throughput Printing of Aligned Nanostructured Polymer Semiconductors for MHz Large-Area Electronics. *Nat. Commun.* **2015**, *6*, 8394.
- (56) Tilley, A. J.; Guo, C.; Miltenburg, M. B.; Schon, T. B.; Yan, H.; Li, Y.; Seferos, D. S. Thionation Enhances the Electron Mobility of Perylene Diimide for High Performance n - Channel Organic Field Effect Transistors. *Adv. Funct. Mater.* **2015**, *25*, 3321–3329.
- (57) Chen, W.; Zhang, J.; Long, G.; Liu, Y.; Zhang, Q. From Non-Detectable to Decent: Replacement of Oxygen with Sulfur in Naphthalene Diimide Boosts Electron Transport in Organic Thin-Film Transistors. *J. Mater. Chem. C* **2015**, *3*, 8219–8224.
- (58) Kozycz, L. M.; Guo, C.; Manion, J. G.; Tilley, A. J.; Lough, A. J.; Li, Y.; Seferos, D. S. Enhanced Electron Mobility in Crystalline Thionated Naphthalene Diimides. *J. Mater. Chem. C* **2015**, *3*, 11505–11515.
- (59) Welford, A.; Maniam, S.; Gann, E.; Thomsen, L.; Langford, S. J.; McNeill, C. R. Thionation of Naphthalene Diimide Molecules: Thin-Film Microstructure and Transistor Performance. *Org. Electron.* **2018**, *53*, 287–295.
- (60) Pahlavanlu, P.; Tilley, A. J.; Mcallister, B. T.; Seferos, D. S. Microwave Synthesis of

- Thionated Naphthalene Diimide-Based Small Molecules and Polymers. *J. Org. Chem.* **2017**, *82*, 12337.
- (61) Shin, Y.; Welford, A.; Komber, H.; Matsidik, R.; Thurn-Albrecht, T.; McNeill, C. R.; Sommer, M. Regioregular Polymer Analogous Thionation of Naphthalene Diimide – Bithiophene Copolymers. *Macromolecules* **2018**, *51*, 984–991.
- (62) Luzio, A.; Fazzi, D.; Natali, D.; Giussani, E.; Baeg, K. J.; Chen, Z.; Noh, Y. Y.; Facchetti, A.; Caironi, M. Synthesis, Electronic Structure, and Charge Transport Characteristics of Naphthalenediimide-Based Co-Polymers with Different Oligothiophene Donor Units. *Adv. Funct. Mater.* **2014**, *24*, 1151–1162.
- (63) Fazzi, D.; Caironi, M.; Castiglioni, C. Quantum-Chemical Insights into the Prediction of Charge Transport with Enhanced Electron Mobility. *J. Am. Chem. Soc.* **2011**, *133*, 19056–19059.
- (64) Wang, S.; Sun, H.; Ail, U.; Vagin, M.; Persson, P. O. A.; Andreasen, J. W.; Thiel, W.; Berggren, M.; Crispin, X.; Fazzi, D.; Fabiano, S. Thermoelectric Properties of Solution-Processed n-Doped Ladder-Type Conducting Polymers. *Adv. Mater.* **2016**, *28*, 10764–10771.
- (65) Shin, Y.; Massetti, M.; Komber, H.; Biskup, T.; Nava, D.; Lanzani, G.; Caironi, M.; Sommer, M. Improving Miscibility of a Naphthalene Diimide-Bithiophene Copolymer with n-Type Dopants through the Incorporation of “Kinked” Monomers. *Adv. Electron. Mater.* **2018**, *1*, 1700581.
- (66) Kiefer, D.; Giovannitti, A.; Sun, H.; Biskup, T.; Hofmann, A.; Koopmans, M.; Cendra, C.; Weber, S.; Anton Koster, L. J.; Olsson, E.; Rivnay, J.; Fabiano, S.; McCulloch, I.; Müller,

- C. Enhanced N-Doping Efficiency of a Naphthalenediimide-Based Copolymer through Polar Side Chains for Organic Thermoelectrics. *ACS Energy Lett.* **2018**, *3*, 278–285.
- (67) Garcia-belmonte, G.; Munar, A.; Barea, E. M.; Bisquert, J.; Ugarte, I.; Pacios, R. Charge Carrier Mobility and Lifetime of Organic Bulk Heterojunctions Analyzed by Impedance Spectroscopy. *Org. Electron.* **2008**, *9*, 847.
- (68) Bittle, E. G.; Basham, J. I.; Jackson, T. N.; Jurchescu, O. D.; Gundlach, D. J. Mobility Overestimation Due to Gated Contacts in Organic Field-Effect Transistors. *Nat. Commun.* **2016**, *7*, 10908.
- (69) Africa, P. C.; De Falco, C.; Maddalena, F.; Caironi, M.; Natali, D. Simultaneous Extraction of Density of States Width , Carrier Mobility and Injection Barriers in Organic Semiconductors. *Sci. Rep.* **2017**, *7*, 3803.
- (70) Lu, N.; Li, L.; Liu, M. A Review of Carrier Thermoelectric-Transport Theory in Organic Semiconductors. *Phys. Chem. Chem. Phys.* **2016**, *18*, 19503.
- (71) Lilliu, S.; Agostinelli, T.; Pires, E.; Hampton, M.; Nelson, J.; Macdonald, J. . E. Dynamics of Crystallization and Disorder during Annealing of P3HT / PCBM Bulk Heterojunctions. *Macromol. Symp.* **2011**, *44*, 2725–2734.
- (72) Kirby, N. M.; Mudie, S. T.; Hawley, A. M.; Cookson, D. J.; Mertens, H. D. T.; Cowieson, N.; Samardzic-Boban, V. A Low-Background-Intensity Focusing Small-Angle X-Ray Scattering Undulator Beamline. *J. Appl. Crystallogr.* **2013**, *46*, 1670–1680.
- (73) Ilavsky, J. Nika: Software for Two-Dimensional Data Reduction. *J. Appl. Crystallogr.* **2012**, *45*, 324–328.

(74) Beretta, D.; Massetti, M.; Lanzani, G.; Caironi, M. Thermoelectric Characterization of Flexible Micro-Thermoelectric Generators. *Rev. Sci. Instrum.* **2017**, *88*, 015103.

TOC Graphic

